Extreme interfacial waves

R. H. J. Grimshaw
School of Mathematics, University of New South Wales, Kensington, New South Wales 2033, Australia

D. I. Pullin
Department of Mechanical Engineering, University of Queensland, Queensland 4067, Australia

(Received 3 January 1986; accepted 13 June 1986)

Numerical solutions are presented for large-amplitude interfacial waves of extreme form on the interface between two fluids of different densities in the Boussinesq approximation. The flow in the lower fluid is irrotational, but the upper fluid may have constant, nonzero vorticity. Only symmetric waves are calculated. The results suggest limiting wave profiles for which separate portions of the interface touch, forming stagnant zones of one fluid imbedded in the other fluid.

I. INTRODUCTION

Recently, there has been a revival of interest in the properties of extreme periodic waves of permanent form propagating on the free surface of a homogeneous fluid. Some fascinating results have been obtained, such as the discovery that for fixed wavelength the wave speed and energy are not monotonic properties of wave amplitude (Longuet-Higgins,[1] Longuet-Higgins and Fox[2]), and the existence of bifurcations to various classes of irregular waves (Chen and Saffman[3]). A relatively recent review by Schwartz and Fenton[4] gives a useful summary of these results.

By contrast there has been comparatively little work on the properties of permanent, finite-amplitude waves on the interface between two homogeneous fluids. Holyer[5] used a Stokes expansion and Padé approximants to calculate wave profiles up to a limiting wave which contained a vertical tangent, while her results were confirmed by Vanden-Broeck[6] who obtained numerical solutions of an integral equation formulation. Subsequently Meiron and Saffman[7] established that overhanging, or S-shaped, waves could exist, using numerical methods either based on a Fourier series representation of the wave or based on an integral equation formulation. They also suggested the possibility that the wave speed is not a single-valued function of wave amplitude, and that for the most extreme waves the wave amplitude may decrease as the wave speed increases. Very recently this conjecture has been confirmed by Turner and Vanden-Broeck[8] who showed that for a density ratio of 0.1 the wave speed–wave amplitude curve has a self-intersecting spiral shape and that the wave profile correspondingly oscillates alternating between an S-shape and a single-valued profile. They conjectured that this oscillation continues indefinitely, in analogy with the results of Longuet-Higgins and Fox[2] for water waves. Simultaneously and independently, we, in two papers[9,10] (henceforth denoted as PGI and II, respectively), constructed wave profiles for a variety of basic flow configurations, including some with a finite depth to the upper fluid, linear basic current shear in the upper fluid, and a basic current jump across the interface; this last case has also been considered by Saffman and Yuen.[11] We also found S-shaped waves for some basic flow configurations. Our numerical results were based on an integral equation formulation. However, because our search for very large amplitude waves proceeded in steps of increasing wave amplitude, our results were limited to those solution branches for which other wave properties, such as the wave speed, are single-valued functions of the wave amplitude. We conjectured[10] that in the absence of a constraining upper boundary, the limiting wave was one in which a stagnation point first appeared in the wave profile. This is shown here to be incorrect. A more comprehensive procedure than that used in PGI and II, and one that in principle should locate solution branches for which the wave properties are multivalued functions of wave amplitude, is to search for solutions along the solution curve in wave speed–amplitude space, allowing both these properties as parameters to be determined, and defining a unique solution point by the specification of an arc, or chord, length on the solution curve itself. In this paper we report the results of this approach for the calculation of interfacial waves of extreme form, in which distinct portions of the wave profile nearly come into mutual contact. Wave shapes with similar properties have recently been found by Simmen and Saffman,[12] who studied highly nonlinear progressive waves of permanent form on the free surface of a homogeneous fluid when there is a linear basic current shear in the fluid.

II. FORMULATION

The problem formulation and numerical procedure have been described in detail in PGI and II. However, for the convenience of the reader, and to introduce notation, we shall give a brief account here. We consider periodic progressive waves of permanent form at the interface between two fluids of densities ρ_1 and $\rho_2 > \rho_1$, and where subscripts 1 and 2 refer to fluid properties above and below the interface, respectively. The lower fluid is infinitely deep, but the upper fluid has a mean depth d_1, and may also contain a basic current with constant vorticity ω_1. For a wave of wavelength λ we use nondimensional variables based on the length scales λ/π and the time scale $(\lambda/\pi\alpha g)^{1/2}$, where $\alpha = (\rho_2 - \rho_1)/(\rho_2 + \rho_1)$ is the Boussinesq parameter. Following the notation of PGI and II we use capital letters to denote nondimensional variables. Then with the X axis horizontal, and the Y axis vertical, the complex velocity field at a point $Z = X + iY$ in either fluid is expressed in terms of a distribu-

 0031-9171/86/092802-06$01.90

tion of vortex/source singularities $\gamma(a)$ along the interface, denoted by $Z_c = X_c(a) + iY_c(a)$, where a is an interfacial parameter $(0 < a < \pi)$. Thus we write

$$U - iV = \frac{1}{2\pi i}\int_0^{\pi}\left\{\cot(Z - Z_c')\left[\gamma' - \Omega Y_c'\left(\frac{\partial Z_c'}{\partial a'}\right)\right] - \cot(Z - Z_c'^{*} - 2iD)\left[\gamma' - \Omega Y_c'\left(\frac{\partial Z_c'^{*}}{\partial a'}\right)\right]\right\}da' - A\Omega Y - C, \quad (1)$$

where $A = 1, 0$ according as Z lies in the upper, or lower, fluid, and where dashed quantities are all functions of a'. Here $D = d_1\pi/\lambda$, $\Omega = \omega_1(\lambda/\pi a g)^{1/2}$, C is the nondimensional wave speed, and $\gamma(a)$ is the tangential velocity jump across the interface. Note that (1) corrects a typographical error in the equivalent Eq. (16) of PGII where the term C was omitted. In the Boussinesq limit, $\alpha \to 0$, the boundary conditions at the interface may be written as

$$\gamma\left(\frac{\partial Z_c^{*}}{\partial a}\right)^{-1}(U - iV)_p + 2Y_c = \text{const.} \quad (2)$$

In this expression $(U - iV)_p$ is the mean of the generally unequal fluid velocities on either side of the interface, and is obtained from (1) (the first term is then a Cauchy principal value integral). There are three remaining constraints, relating to the circulation, the mean interface level, and the wave amplitude δ. These are

$$\int_0^{\pi}\gamma(a)da = 0, \qquad \int_0^{\pi} Y_c\frac{\partial X_c}{\partial a}da = 0, \quad (3)$$

and

$$Y_{c_{\max}} - Y_{c_{\min}} = 2\delta.$$

The basic state parameters are thus D and Ω, and the wave parameters are C and δ.

The numerical procedure used here follows that developed in PGI and II. Thus we put

$$Z_c(a) = a + \sum_{n=0}^{N=1}[A_n \sin(2na) + iB_n \cos(2na)], \qquad \gamma(a) = \sum_{1}^{N} E_n \cos(2na), \quad (4)$$

where we assume that the wave shape is symmetrical about the crest $(a = 0)$ and the trough $(a = \pi/2)$. These expressions are substituted into (1) and (2) and evaluated at the $N + 1$ points $a_n = n\pi/2N$, $n = 0,...,N$. The numerical treatment of the integals is described in PGI. The parameter a is chosen to allow computation of very steep waves. We further introduce a set of chord length equations

$$|Z_c(a_n) - Z_c(a_{n-1})| = (\epsilon\pi/2N)\{1 + \tfrac{1}{2}\beta[\cos(2a_n) + \cos(2a_{n-1})]\}, \quad n = 1,...,N, \quad (5)$$

where $\beta(0 < \beta < 1)$ is a specified parameter and ϵ is an unknown. We now close the system of nonlinear equations in the following way. All parameters are specified as functions $A_n(s)$, $B_n(s)$, $E_n(s)$, $\epsilon(s)$, $C(s)$, and $\delta(s)$ of the variable s, which is an arc length on the $(C - C_0)$ vs δ curve, such that $\Delta s^2 = [\Delta(C - C_0)]^2 + \Delta\delta^2$ and $s = 0$ for $C - C_0 = 0$, $\delta = 0$. Hence s is monotonically increasing on the $(C - C_0)$ vs δ curve, for $\delta > 0$, and is continuous provided the solution branch is continuous. Introducing a constraint fixing s then gives $3N + 3$ equations for the $3N + 3$ unknowns A_n, B_n, E_n, ϵ, C, and δ. We note that the size of this system could be reduced by defining a new parameter $\Delta b = \gamma(a)\Delta a$ and specifying $Z_c = Z_c(b)$, thus eliminating γ altogether. However, in practice this more compact scheme suffers from the major disadvantage that it will fail, should, as occurs presently, $\gamma(a)$ nearly vanish along finite portions of the interface, for then $Z_c(b)$ would be nearly discontinuous, and this is difficult to handle numerically.

The Newton–Raphson iterative scheme was used to solve the set of nonlinear equations as follows: Families of solutions are defined by fixing the basic state parameters D and Ω. Assume a set of solutions is known for arc lengths $s_j = 0,...,J$. A new solution is then sought which is the intersection of $(C - C_0)$ vs δ curve with an appropriate arc of the circle

$$(C_{J+1} - C_J)^2 + (\delta_{J+1} - \delta_J)^2 = (s_{J+1} - s_J)^2, \quad (6)$$

where s_{J+1} is specified. An initial guess was obtained from a linear, or higher-order, extrapolation in s from the solutions $s_J, s_{J-1},...$. If the iteration scheme did not converge such that the mean residual was at most $O(10^{-8})$ in 14-figure arithmetic, $s_{J+1} - s_J$ was halved, and the process repeated.

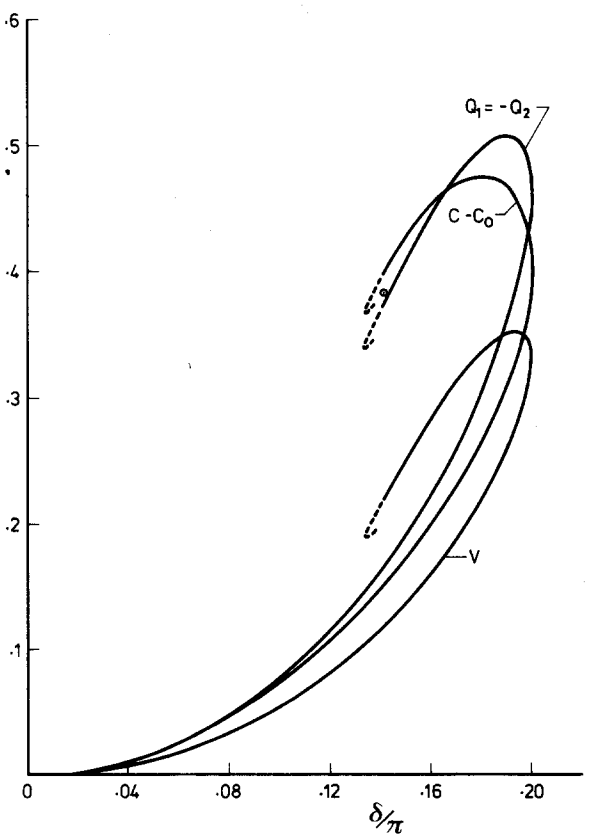

FIG. 1. Wave speed $C - C_0$, excess x-wise volume flux in layer j, Q_j, and potential energy per wavelength V, $D \to \infty$, $\Omega = 0$. ⊙ $C - C_0$, δ/π, limiting water wave.

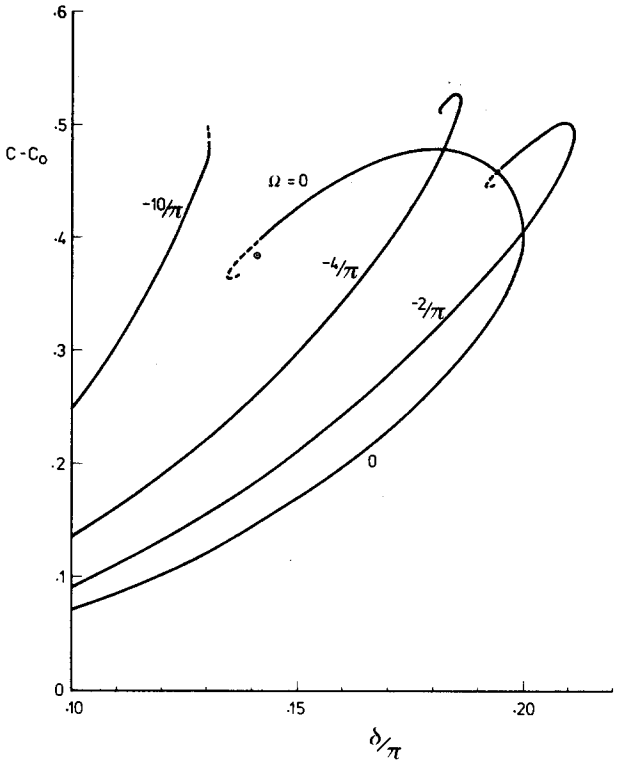

FIG. 2. Wave speed $C - C_0$, $D \to \infty$. Values of Ω as shown. ⊙ Limiting water wave, $\Omega = 0$.

The search for solutions was terminated when five successive halvings produced no new solution. We denote this most extreme wave by δ_{ex} and C_{ex}, which is apparently the limit that can be achieved by this numerical method. Note that we distinguish this wave from the hypothetical limiting wave denoted by δ_{lim}, C_{lim}, which will be discussed subsequently. Once a set of solutions (for fixed D and Ω) had been obtained, usually with $N = 70$ (points per half-wavelength), a subset was calculated with $N = 100$ or 130, to check for sensitivity to N. Solutions which we consider reliable showed a four to five figure agreement for wave properties (e.g., C), with $N = 70$, 130. This range is indicated by the solid curves in Figs. 1–3, while the dashed portions of the curves indicate sensitivity to N. At the limit of reliability the ratio of the magnitude of the last few Fourier coefficients in (4) to the maximum coefficient was typically $O(10^{-4})$. The onset of sensitivity to N for $N \geqslant 70$ was accompanied by a rapid increase in this ratio, which appeared first as oscillations in γ. There are two reasons for the ultimate failure of the numerical method. First, very slow convergence of (4) caused by the extreme wave profile. Second, the mutual approach of two distinct portions of the interface, seen in Figs. 4–8, leads to nearly singular behavior of the integrands in (1) which was not specifically resolved analytically (see PGI and II) prior to implementation of the numerical method.

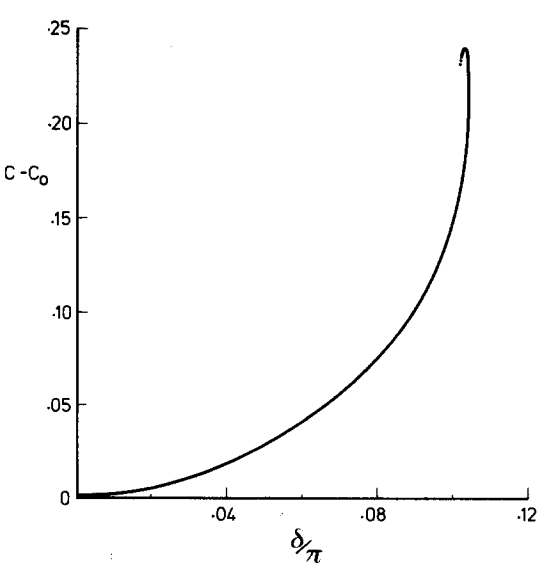

FIG. 3. Wave speed $C - C_0$, $D = 0.1\pi$, $\Omega = 0$.

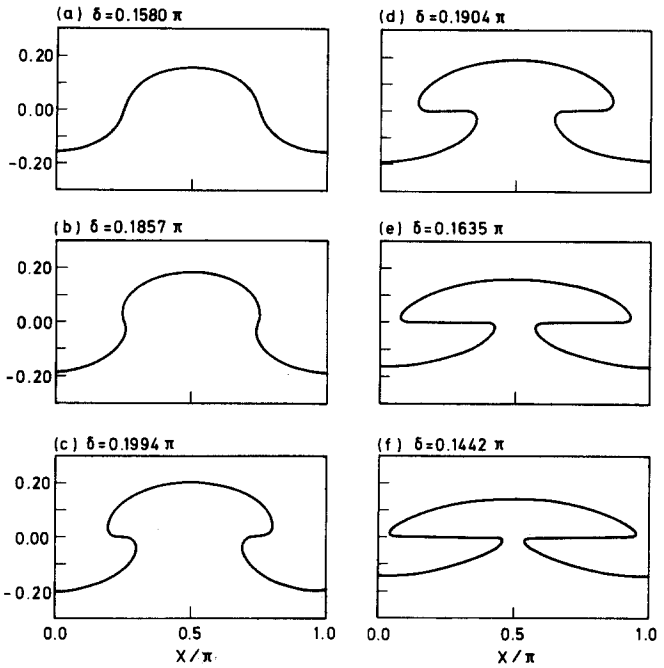

FIG. 4. Wave profiles, $D \to \infty$, $\Omega = 0$. Values of δ as shown.

III. RESULTS

The numerical results are shown in Figs. 1–8. Figures 1 and 2 show a plot of wave speed as a function of wave amplitude for the case when the upper fluid is infinitely deep ($D \to \infty$) and for various values of basic current shear Ω. All curves show a tendency to spiral passing through first a point of maximum wave amplitude δ_{max}, then through a point of

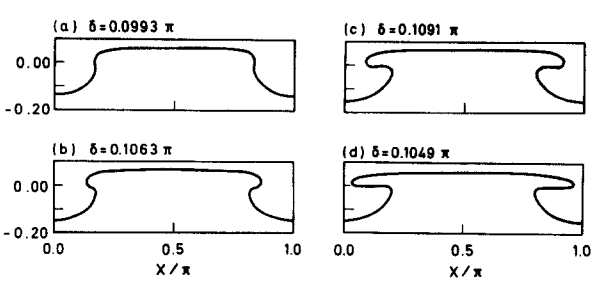

FIG. 5. Wave profiles, $D = 0.1\pi$, $\Omega = 0$. Values of δ as shown.

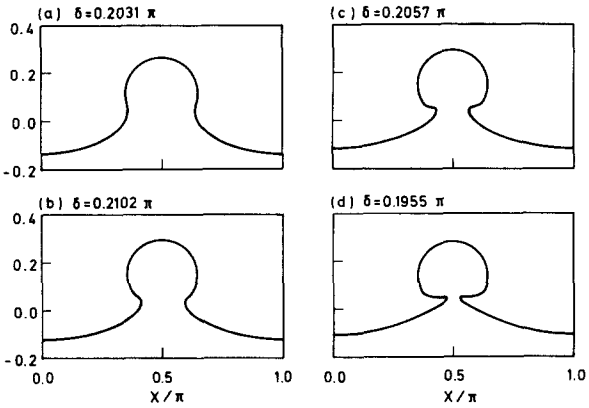

FIG. 6. Wave profiles, $D\to\infty$, $\Omega = -2/\pi$. Values of δ as shown.

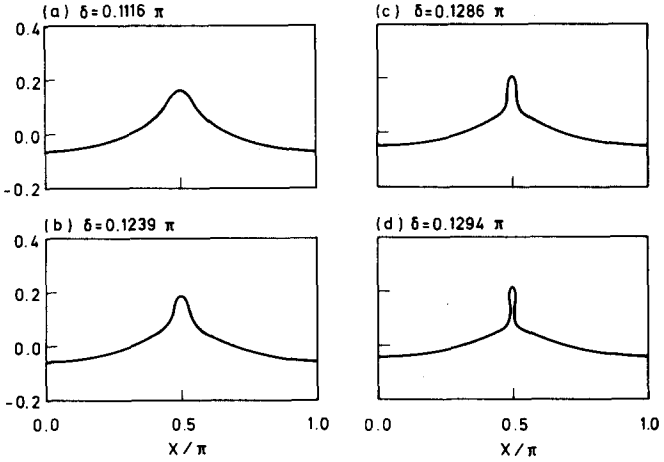

FIG. 8. Wave profiles, $D\to\infty$, $\Omega = -10/\pi$. Values of δ as shown.

maximum wave speed $C_{\max}$, and ultimately reaching the extreme waves, δ_{ex} and C_{ex}. The spiral is most pronounced for the case $\Omega = 0$, which is the case of most interest, corresponding to waves on the interface between two infinitely deep fluids. Other wave properties show a similar trend, and some of these are shown in Fig. 1 for the case $\Omega = 0$, $D\to\infty$. Similar results are also obtained when the upper layer has finite depth, and one such case is shown in Fig. 3 for $D/\pi = 0.1$ and $\Omega = 0$.

The corresponding wave shapes over a full wavelength are shown in Figs. 4–8. First consider Fig. 4 which shows the case $D\to\infty$ and $\Omega = 0$ for a range of values of wave amplitude. The corresponding wave speeds are shown in Fig. 2. This case can be regarded as a continuation of the wave shape calculations reported in PGII (Fig. 1). As the wave speed–wave amplitude curve is traversed the wave shape passes through the sequence of cases (a)–(f). The wave first develops an S shape, which becomes more pronounced as the sequence progresses until we reach the mushroom-shaped wave in case (f). It is remarkable that the values $\delta = 0.1442\pi$ and $C = 1.116$ for case (f) (the last reliable result we could obtain) agree quite closely with the values $\delta_{\lim} = 0.1411\pi$ and $C_{\lim} = 1.0923$ for the limiting water wave, which has the 120° angle at its crest (see for instance, Longuet-Higgins[1] or Williams[13]). The agreement is even closer if we are prepared to accept the dashed portions of the curves in Figs. 1 or 2. This leads us to conjecture that the limiting interfacial wave consists of a pair of limiting water waves, that for the upper fluid being inverted, and separated by a region of stagnant fluid. The conjectured configuration is shown in Fig. 9. It is significant that since the region between the two water wave profiles is stagnant, the configuration shown is an exact solution of the governing equations. After taking account of the nondimensionalization, each wave profile is an exact solution of the water wave equations for the case of the limiting wave (the existence of this solution with the 120° crest has recently been established by Amick, Fraenkel, and Toland[14]). Of course, this conjectured limiting shape, together with all the S-shaped waves are presumably convectively unstable due to the presence of some heavier fluid (density ρ_2) overlying the lighter fluid (density ρ_1). However, questions of existence are separate from those of stability, and we emphasize that the configuration shown in Fig. 9 is an exact solution. This leads us to conjecture that all the wave shapes shown in Fig. 4 correspond to exact solutions of the governing equations.

Further, Longuet-Higgins and Fox[2] in their calculation of water waves found that the wave speed–wave amplitude curve oscillates indefinitely as the limiting wave is approached. This suggests that the same behavior may occur here, but was not detected explicitly by us because the numerical method failed when the wave profile assumed a "nearly touching" shape. Very recently Turner and Vanden-Broeck[8] have shown that for the case $\alpha = 0.818$ the wave

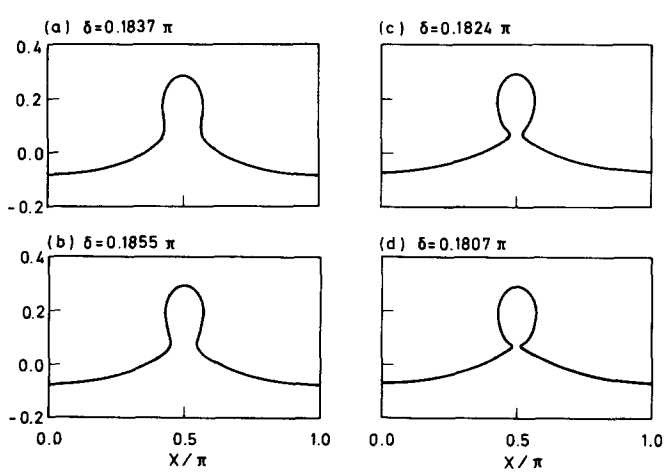

FIG. 7. Wave profiles, $D\to\infty$, $\Omega = -4/\pi$. Values of δ as shown.

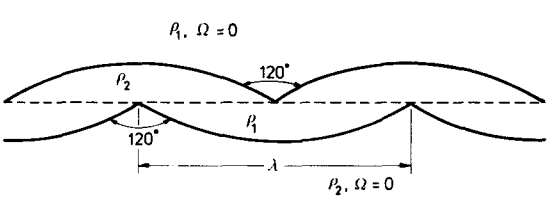

FIG. 9. Conjectured limiting wave profile, $D\to\infty$, $\Omega = 0$. Each solid line is a limiting water wave profile.

speed–wave amplitude curve has a self-intersecting shape, and the wave profile oscillates indefinitely. However, their wave profiles alternate between an S shape, and a single-valued profile, and there is no evidence for a nearly touching profile. It is relevant to note here the curious fact that for this case $\Omega = 0$ there is a family of exact detached solutions, for each of which the upper fluid is separated from the lower fluid by a stagnant zone, and the wave profile for each fluid is an exact solution of the water wave equations, after taking account of the nondimensionalization. The limiting wave shown in Fig. 9 is one member of this family. Of course, the wave speeds corresponding to each profile must agree, and this places some constraint on the values of wave amplitude δ, and the densities ρ_1, ρ_2, or the mean depths d_1, d_2, for which this solution is a possibility. Note also that for $\rho_1 \neq \rho_2$, or $d_1 \neq d_2$, the wave profiles for the upper and lower fluids differ from each other. For the case $d_1, d_2 \to \infty$ it can be shown that this restricts $\alpha < 0.214$. We note that $\alpha = 0.818$, the value used by Turner and Vanden-Broeck,[8] lies outside this range, and thus these detached solutions cannot be found in their calculations.

Next consider Fig. 5 which shows the case $D = 0.1\pi$ and $\Omega = 0$ for a range of values of wave amplitude. The corresponding wave speeds are shown in Fig. 3. This case can be regarded as a continuation of the wave shape calculations reported in PGI (Fig. 1). The general pattern is similar to that for the case $D \to \infty$ and $\Omega = 0$ although we were unable to obtain results very close to the conjectured values of δ_{lim} and C_{lim} because of the occurrence of high-frequency noise in the numerical scheme. Generally, as D is decreased a larger number of Fourier components (i.e., a larger value of N) is required.

Wave shapes for $\Omega \neq 0$ are shown in Figs. 6–8; all cases are for $D \to \infty$. Figure 6 can be regarded as a continuation of the wave shape calculations reported in PGII (Fig. 2). The general pattern as the wave speed–wave amplitude curve is traversed is initially similar to that for the case $\Omega = 0$, but shows considerable differences as δ_{lim} is approached, the differences being accentuated as $|\Omega|$ increases. The conjectured configuration for the limiting wave, δ_{lim}, cannot be described by Fig. 9, as with $\Omega \neq 0$ it is not possible to form a zone of stagnant fluid separating the two fluids. Instead, we conjecture that the limiting wave may adopt the configuration shown in Fig. 10. Each wave has a crest angle of 120° containing the lower fluid of density ρ_2 and zero vorticity ($\Omega = 0$). On top of the crest sits a "bubble" of the lower fluid in which the flow is stagnant; at the point of contact of the bubble and the wave crest, the bubble boundary is locally horizontal. A local analysis near the wave crest similar to that for the free-surface Stokes wave shows that this configuration is allowed. The stream function Ψ in the lower fluid has a leading term of $\frac{2}{3}\sqrt{2}r^{3/2}\cos(3\theta/2)$, where r is the distance from the wave crest, and θ is the polar angle measured from the downward vertical, while $\Psi = 0$ in the bubble. In the upper fluid the leading term for Ψ is $\frac{1}{4}\Omega r^2[-1 \pm (2/\sqrt{3})\sin 2(\theta \mp \pi/6)]$, where the alternate signs refer to the regions to the right and left of the crest, respectively. Thus relative to the lower fluid, the upper fluid is locally stagnant. The bubble boundary near the wave crest

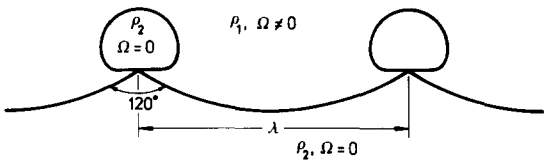

FIG. 10. Conjectured limiting wave profile, $D \to \infty$, $\Omega \neq 0$.

is locally horizontal but has curvature proportional to Ω [Y is $O(\Omega r^2)$]. As the vorticity $|\Omega|$ is decreased, the bubble region expands and the flow in the upper fluid weakens until the limiting configuration of Fig. 9 is reached. For instance, compare the configurations shown in Fig. 4(f) with that in Fig. 6(d). On the other hand as $|\Omega|$ increases, the bubble region contracts [compare Figs. 7(d) and 8(d)] and the flow in the upper fluid strengthens with the consequence that the curvature of the bubble at the crest increases. For large values of $|\Omega|$ the bubble will be extremely difficult to detect and the wave profile will appear to have developed a 120° corner (see Figs. 3 and 10 of PGII for an example of this when $\Omega = -100/\pi$). Note, however, that for very large values of $|\Omega|$ the leading order term in the lower fluid (where Ψ is proportional to $r^{3/2}$) will dominate over the leading order term in the upper fluid (where Ψ is proportional to Ωr^2) only for r of $O(\Omega^{-2})$, with the consequence that the crest angle will only be apparent within this small zone. For instance, in Fig. 3 of PGII, r must be less than 2×10^{-2} before the limiting configuration is apparent. As $|\Omega| \to \infty$ (i.e., neglecting the effects of gravity completely) Broadbent and Moore[15] have conjectured that the crest angle is 90° with no enclosed bubble. As they point out it follows that for large, but finite, values of $|\Omega|$ the crest angle may appear to be 90° on a coarse scale, but finally adopting a 120° angle for r of $O(\Omega^{-2})$. There is some evidence for this behavior in Fig. 3 of PGII, and also in the work of Simmen and Saffman[12] who calculated wave profiles on the free surface of a homogeneous fluid when there is constant vorticity in the fluid.

IV. DISCUSSION

For each of the five (D,Ω) parameter sets studied here, the wave profiles correspond to a continuous progression along the $(C - C_0)$ vs δ curve from the flat, undisturbed interface towards an apparent limit, not explicitly resolved, in which distinct portions of the interface come into contact thus forming closed and stagnant zones of one fluid imbedded within the other fluid. We cannot conclude, however, that each (D,Ω) solution set, containing perhaps this extreme limiting wave, is complete since the possibility remains that there exist further solution branches that cannot be reached by our present numerical method. These may include solutions with bubble zones different from those shown in Figs. 9 and 10 for the conjectured limiting waves, or solutions in which the bubble zone reopens, or combinations of both of these possibilities. For example, Simmen and Saffman,[12] in their numerical calculation of highly nonlinear waves on the free surface of a homogeneous fluid with constant vorticity, found that for sufficiently large and positive vorticity, the solution branches contained gaps in the

$(C - C_0)$ vs δ curves, with the end points of the gaps bounded by two different, but nearly touching wave profiles. Indeed, their nearly touching profiles bear some resemblance to those calculated by us when viewed from the upper fluid [e.g., see Figs. 6(d), 7(d), and 8(d), and reverse the Y axis]. However, in the configuration studied by Simmen and Saffman[12] the entire upper fluid (i.e., our lower fluid) is stagnant, and consequently the local solution for a bubble zone would be unlike that shown in Fig. 10.

[1]M. S. Longuet-Higgins, Proc. R. Soc. London Ser. A **342**, 157 (1975).
[2]M. S. Longuet-Higgins and M. J. H. Fox, J. Fluid Mech. **85**, 769 (1978).
[3]B. Chen and P. G. Saffman, Stud. Appl. Math. **62**, 1 (1980).
[4]L. W. Schwartz and J. D. Fenton, Annu. Rev. Fluid Mech. **14**, 39 (1982).
[5]J. Y. Holyer, J. Fluid Mech. **93**, 433 (1979).
[6]J-M. Vanden-Broeck, Phys. Fluids **23**, 1723 (1980).
[7]D. I. Meiron and P. G. Saffman, J. Fluid Mech. **129**, 213 (1983).
[8]R. E. L. Turner and J-M. Vanden-Broeck, Phys. Fluids **29**, 372 (1986).
[9]D. I. Pullin and R. H. J. Grimshaw, Phys. Fluids **26**, 897 (1983).
[10]D. I. Pullin and R. H. J. Grimshaw, Phys. Fluids **26**, 1731 (1983).
[11]P. G. Saffman and H. C. Yuen, J. Fluid Mech. **123**, 459 (1982).
[12]J. Simmen and P. G. Saffman, Stud. Appl. Math. **73**, 35 (1985).
[13]J. M. Williams, Philos. Trans. R. Soc. London Ser. A **302**, 139 (1981).
[14]C. J. Amick, L. E. Fraenkel, and J. F. Toland, Acta. Math. **148**, 193 (1982).
[15]E. G. Broadbent and D. W. Moore, Phys. Fluids **28**, 1561 (1985).